7th International Conference on Silicon Photovoltaics, SiliconPV 2017

Radiative recombination coefficient in crystalline silicon at low temperatures < 77 K by combined photoluminescence measurements

Rudolf Brüggemann*, Ming Xu, José Alvarez, Mohamed Boutchich, Jean-Paul Kleider

GeePs (Group of Electrical Engineering - Paris), UMR CNRS 8507, CentraleSupélec, Univ. Paris-Sud, Université Paris-Saclay, Sorbonne Universités, UPMC Univ Paris 06, 11 rue Joliot-Curie, Plateau de Moulon, F-91192 Gif-sur-Yvette Cedex, France

Abstract

Spectral photoluminescence (sPL) and modulated photoluminescence (MPL) measurements were applied to determine the band-to-band radiative recombination coefficient, B_{rad}, in crystalline silicon. We used precursors of n-type crystalline silicon solar cells consisting of two different wafers passivated with aluminum oxide stacks or intrinsic hydrogenated amorphous silicon, respectively. So far values for B_{rad} can be found in the literature only above 77 K. In this high-temperature range the temperature dependence of B_{rad} obtained using our combined sPL/MPL method is in good agreement with the available literature data for both samples. Interestingly, we have extended the measured range down to a temperature of 20 K and observed a strong increase of B_{rad} by three orders of magnitude with decreasing temperature from 77 K to 20 K.

Keywords: silicon; radiative recombination; recombination coefficient; photoluminescence

1. Introduction

The temperature dependence of the radiative recombination coefficient B_{rad} for crystalline silicon (c-Si) is described in a number of publications for a temperature range between 77 K and 393 K [1-3]. The theory by Ruff *et al.* [4] describes this temperature dependence qualitatively with almost constant values in the range between about

* Corresponding author.
  E-mail address: rudi.brueggemann@geeps.centralesupelec.fr

400 K and 250 K and with increasing values of B_{rad} with further decreasing temperature T. In this paper, we determine B_{rad} in c-Si at low temperatures between 20 K and 77 K for which no data are available. The measurement range also covers measurements from 77 K up to 315 K for comparison and calibration with the literature data. The results are achieved by a combination of stationary spectral photoluminescence (sPL) and modulated photoluminescence (MPL) [5]. The elegance of the method results from the possibility of determining B_{rad} without the need of precise data for the T-dependent absorption coefficient or the intrinsic carrier density. With respect to characterization and numerical simulation of experiments, the knowledge of the low-T radiative coefficient data complements the background information that may form the base for the interpretation of photoluminescence or electroluminescence experiments for characterization, should they be extended to lower T.

2. Experimental and evaluation methods

Trupke *et al.* [1] outlined that the energy-dependent spectral radiative recombination coefficient $B_{rad,s}$ may be determined from the energy-dependent absorption coefficient α_{BB} for band-to-band transitions and other quantities. Integrating appropriately over energy $\hbar\omega$ leads to the total radiative recombination coefficient B_{rad} as

$$B_{rad}(T) = \int B_{rad,s}(T,\hbar\omega)\, d\hbar\omega. \tag{1}$$

The spectral sPL-photon flux emitted from a sample surface can be shown to be given by [1,6,7]

$$B_{rad,s} d\hbar\omega = \frac{d\, j_{PL}(T,\hbar\omega)}{np} \frac{4\, \alpha_{BB}(T,\hbar\omega)\, n_r^2(T,\hbar\omega)}{A(T,\hbar\omega)} \tag{2}$$

where $d\, j_{PL}(T,\hbar\omega)$ is the spectral PL photon flux in the energy interval $d\hbar\omega$, n and p represent the densities of the recombining species via the free electron and hole densities in the bands, n_r is the refractive index and A the absorption. The absorption term A [8] can be simplified under the assumption that only band-to-band transitions are relevant and that $\alpha_{BB} d < 1$ holds, where d is the sample thickness. The derived expression [9]

$$B_{rad,s} d\hbar\omega = \frac{d\, j_{PL}(T,\hbar\omega)}{np} \frac{4\, n_r^2}{C_{ref}\, d} \tag{3}$$

contains only almost temperature independent variables in the second term on the right.

According to Eq. (1), B_{rad} is determined from integrating Eq. (3). With extraction of the variables independent or almost independent on $\hbar\omega$, the definition of $K = 4\, n_r^2 / (C_{ref}\, d)$ and the integrated PL photon flux $J_{PL}(T)$ from

$$J_{PL}(T) = \int d\, j_{PL}(T,\hbar\omega) \tag{4}$$

the derived expression for B_{rad} can be related to the measured signal S via

$$B_{rad}(T) \approx \frac{J_{PL}(T)}{np} K = \frac{K' S(T)}{\left[\Delta n(T) + n_0(T)\right]\Delta p(T)} K. \tag{5}$$

In Eq. (4), the measured signal S is related to $J_{PL}(T)$ by a constant setup-related factor K' and the carrier densities n and p are expressed by the relevant excess carrier densities Δn and Δp and the thermal density n_0. Introducing a calibration factor c defined by the product $K'K = c$ in Eq. (5) gives

$$B_{\text{rad}}(T) = \frac{c\, S(T)}{\left[\Delta n(T) + n_0(T)\right]\Delta p(T)}.$$ (6)

Eq. (6) can be used for determining B_{rad}.

The excess carrier densities can be determined experimentally from MPL [5,10]. The generation rate $G(t)$ in this experiment is modulated sinusoidally with bias dc generation rate G_D and with amplitude G_A according to

$$G(t) = G_D + G_A \exp(i\omega t),$$ (7)

which results in a modulation in excess carrier density $\Delta n(t)$ described by the Ansatz

$$\Delta n(t) = \Delta n_D + \Delta n_A \exp(i\omega t).$$ (8)

Here, the bias density Δn_D defines the recombination lifetime τ via

$$G_D = \Delta n_D / \tau.$$ (9)

From the phase shift φ between excitation and PL emission, related to the complex Δn_A, an MPL-lifetime τ_{MPL} is determined experimentally from

$$\varphi = -\text{atan}(\omega \tau_{MPL}).$$ (10)

If τ does not depend on G_D, then $\tau_{MPL} = \tau$ and the excess carrier density $\Delta n_D(T)$ determined from Eq. (9) can be used, and, equating Δn_D with Δp_D, inserted for Δn and Δp in Eq. (6). The missing $n_0(T)$ can be calculated from the doping density, by taking the temperature dependence of the ionization of the donors into consideration and charge neutrality with temperature-dependent free carrier densities. This has been detailed in [9] for the phosphorus donor level at 45 meV below the conduction band. All the ingredients for the calculation of B_{rad} are thus available for each measurement temperature. It is noted that a precise knowledge of the *T*-dependent absorption coefficient $\alpha_{BB}(T)$ or the intrinsic carrier density $n_i(T)$ is not necessary, thus eliminating two possible error sources. The possible error that is introduced if τ_{MPL} and τ are not equal will be dealt with together with the presentation and discussion of the results.
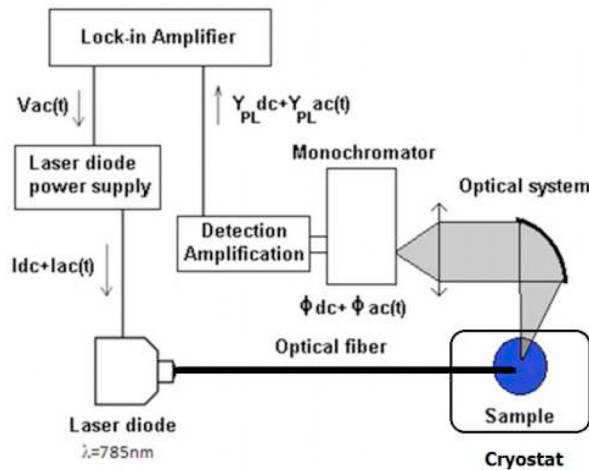

Fig. 1. Experimental setup for the combined measurements of MPL and sPL (Y_{PL} denotes the PL yield, Φ the excitation photon flux and I the current for driving the laser diode). The parabolic mirror collects the PL emission in perpendicular direction from the sample surface.

3. Experimental setup

Fig. 1 sketches the experimental setup with emphasis on the MPL technique. The spectral photoluminescence is measured in the same setup without making any changes to the excitation beam path so that the bias generation rate G_D for MPL corresponds to the steady-state photogeneration rate for the spectral PL measurements, taken from the same excitation spot on the sample and consecutively at each measurement temperature before moving to the next temperature for the following measurement sequence of MPL and sPL.

The figure illustrates that the sample in a closed-cycle He cryostat, which allows cooling down to 20 K, is illuminated by a 785-nm laser diode through the cryostat window using an optical fiber. The laser power is measured with an Ophir Nova II photometer at the position of the sample. The emitted luminescence is collected in reflection mode by a parabolic mirror and focused with an optical lens onto the monochromator entrance. The optics part is a 4f system with a magnification of one. A high-pass optical filter (not shown in the figure) is placed in front of the monochromator to filter the reflected or scattered excitation light. The detection and amplification part consists of an InGaAs photodiode at the monochromator exit and a suitable amplification with a FEMTO current amplifier that delivers voltage to the entrance of a Stanford Research SR830 lock-in amplifier or, in solely DC mode, to a Keithley 195 digital multimeter. For sPL, the modulation is switched off. For the MPL, a sinusoidal output signal of the lock-in amplifier modulates the laser-diode current. Test measurements were performed at 300 K with fixed G_D and a variation of G_A in order to check that the MPL signal was sufficiently high and that the MPL phase was independent of G_A. Low laser-power excitation values in the range of 0.5 and 1 mW cm^{-2} were applied and MPL and sPL were performed under photoexcitation of the same spot on a c-Si wafer.

4. Sample properties

Two samples from different c-Si wafers were investigated. Sample A stems from a Cz-Si wafer while sample B is from an Fz-Si wafer. Table 1 summarizes their properties with different thicknesses d, textures, doping in terms of resistivity ρ, and passivation schemes as well as the reflectance R at the excitation wavelength. The SiC layer was only deposited on one side of Sample A because it served as a preparatory layer for a specific contact scheme, processed with other specimens from the deposition run. Sample A is textured, leading to enhanced absorption on the one hand. On the other hand, Sample A is much thinner than Sample B which results in lower absorption and in a better fulfilment of the inequality $\alpha_{BB}d < 1$, which holds for the PL spectra at lower T and in most of their spectral range at higher T.

Table 1. Summary of the two investigated samples.

	sample A	sample B
c-Si	Cz	Fz
d (μm)	130	280
surface	textured	polished
ρ (Ω cm)	9	2.6
passivation	50 nm AlO$_x$ (both sides), SiC on rear side	50 nm intrinsic a-Si:H (both sides)
R @785 nm	0.012	0.38

5. Results and discussion

5.1. Injection dependence of lifetime

The issue of injection dependence of the lifetime and thus possible differences between steady-state lifetime and differential lifetime from MPL is important. For this reason, in Fig. 2 we show first a complementary photoconductance measurement of the injection dependence of the lifetime at 300 K, measured on sample A before it was cut to fit in the cryostat. In the low injection range where PL measurements shown later were acquired we can adjust the dependence of the lifetime upon excess minority carrier density by a power-law fit Δp^β with a β-value of

about 0.14. According to [11], this leads to less than 17% difference between the steady-state lifetime and the differential lifetime as measured by MPL.

Weak injection dependence is also described by Werner *et al.* [12] for aluminum oxide passivation on n-type Cz-Si, which showed a virtually independent effective surface recombination velocity on injection level. A strong dependence at very low injection is observed at lower excess carrier densities, for example Schmidt *et al.* [13]. But also in this publication the injection dependence for densities $> 10^{14}$ cm^{-3} is weak.

Lifetime-carrier density curves have not been measured on sample B before it was cut to fit in the cryostat. However, data on equivalent samples passivated with intrinsic (undoped) a-Si:H show that the dependence is even lower than in aluminum oxide passivated samples. In addition, similar results on c-Si passivated by thick a-Si:H layers can be seen in [14] with weak injection dependence, for effective surface-recombination velocity, which can be translated into a carrier density, in the relevant range. Thus from these data and the weak injection dependence we can expect the MPL lifetime to be very close to the steady-state one.
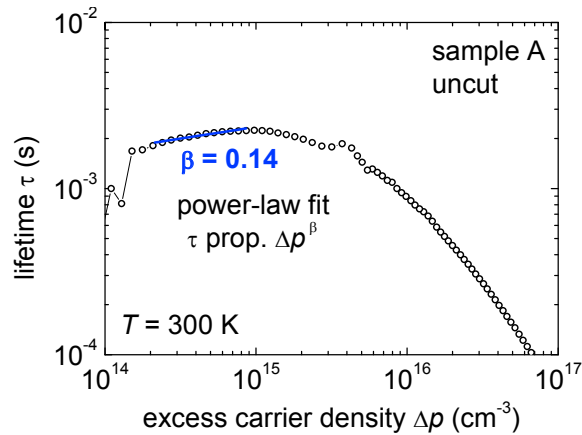

Fig. 2. Lifetime vs. excess carrier density from photoconductance at 300 K. In the injection range of the PL measurements, a power-law fit results in a small value for the exponent β.
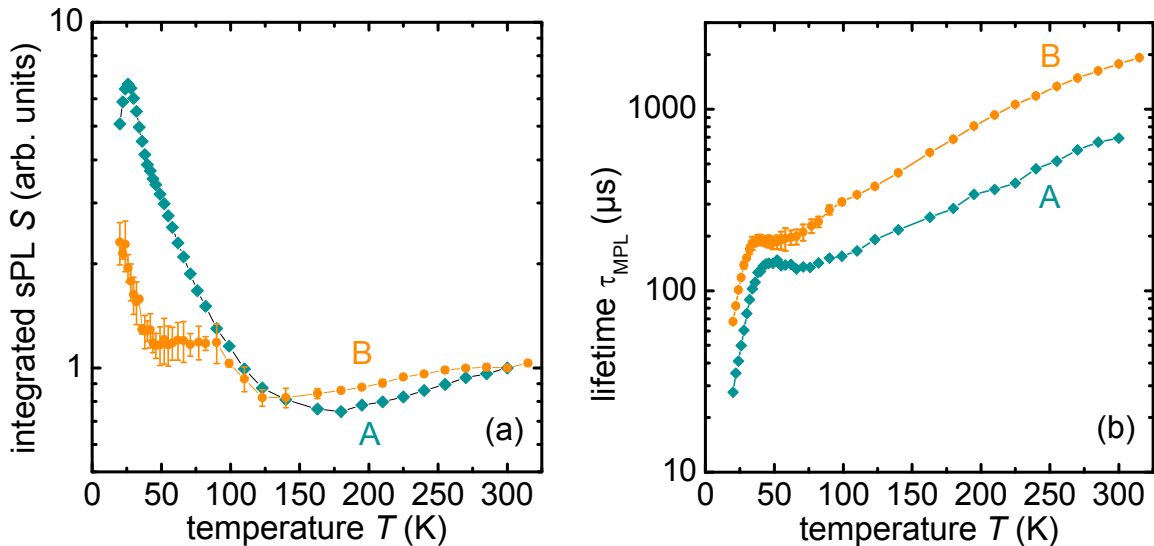

Fig. 3. Temperature dependence of the integrated spectral photoluminescence (a) and of the MPL lifetime (b). Spectral photoluminescence is shown in terms of the integrated signal S on a relative scale, as no absolute determination of the emitted flux is necessary.

5.2. Spectral and modulated photoluminescence

The temperature dependence of the integrated sPL-signal is shown in Fig. 3(a) for samples A and B. They were determined from integration of the spectral PL signal, respectively. The ordinate scale is in arbitrary units as no absolute calibration was carried out because only the relative S values enter in the evaluation. Fig. 3(b) shows the temperature dependence of the MPL lifetime of both samples. Four consecutive runs of the MPL and sPL-measurements were performed for sample B, with two cycles of a 315 K - to - 20 K - to - 315 K sequence, from which the error bars were determined and plotted in Fig. 3. For most of the data points of the mean lifetime for sample B the error bars are smaller than the symbol size.

5.3. Radiative recombination coefficient

The carrier densities $\Delta p(T) = \Delta n(T)$ were determined from the MPL-lifetimes with (9) and the appropriate values for the bias generation rates, and $n_0(T)$-values were calculated from the phosphorus donor level as detailed in [9]. Then relative values of B_{rad} could be determined from Eq. (6). In a next step the calibration constant c is determined so that absolute values of B_{rad} can be obtained. Fig. 4 shows two examples from calibrating to the literatures values given in [1] at either 90 K or 300 K. The overall shape is independent of the choice of calibration. With the choice of plotting B_{rad} on a log-scale vs. temperature a very weak or weak temperature dependence > 100 K is observed, with the present results following the trend in the literature, and a strong increase in B_{rad} values with decreasing temperature at $T < 100$ K.

The determined B_{rad} values for the two samples A and B are close together over the whole temperature range. Fig. 5 details and compares the relative errors of the B_{rad} values of the two samples upon the two calibration procedures with different values of c. At the calibration points 90 K and 300 K the relative error is zero. It is less than 20 % for most of the data points and increases to values in the range of ±40 % at temperatures around 50 K.
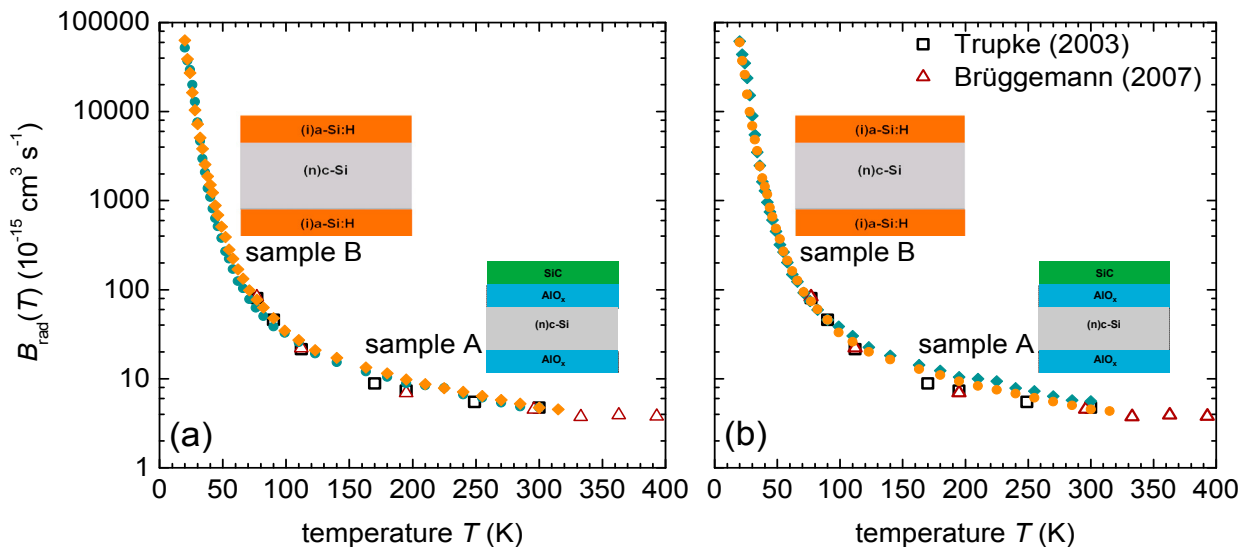

Fig. 4. Determined B_{rad} values for the two samples A and B together with data from [1] and [2]. The absolute B_{rad} values are based on calibration with data from [1] at 300 K in (a) and at 90 K in (b).

At this stage we come back to the discussion on the possible difference between the lifetime from MPL as a differential lifetime and the steady-state lifetime. As discussed in section 5.1, one can expect deviations between differential and steady-state lifetime to be less than 20 % for sample A and much less for sample B at room temperature. Anyhow, if the ratio of differential lifetime and steady-state lifetime was not equal to unity but constant in temperature, Eq. (6) will care that this ratio is absorbed in the factor c, which would not introduce an additional

error over the whole temperature range. Should the ratio be temperature dependent, which is unknown, there would be an error that is introduced in the determination of B_{rad}. Such an error may well account for the 20 % observed variation between literature values and those from the present method for either calibration at 300 K or at 90 K. It may also contribute to the differences in the B_{rad} values determined from the two samples. However, it is noted that at low temperatures the large variation and strong increase in temperature dependence of B_{rad}, both for calibration at 300 K and at 90 K, is expected to be quite well above any error from a possibly temperature dependent ratio of MPL lifetime and steady-state lifetime.

Also, despite the different properties of the two wafer samples with respect to deposition, thickness, wafer doping and passivation-layer related properties like the influence of surface charge [15], good agreement is achieved for the two sets of B_{rad}-data, despite the accounted differences in Fig. 5 of maximal about 40 % around 50 K but with better agreement of < 15 % at most temperatures higher and lower than 50 K for the 300-K calibration and slightly different values for the 90-K calibration.
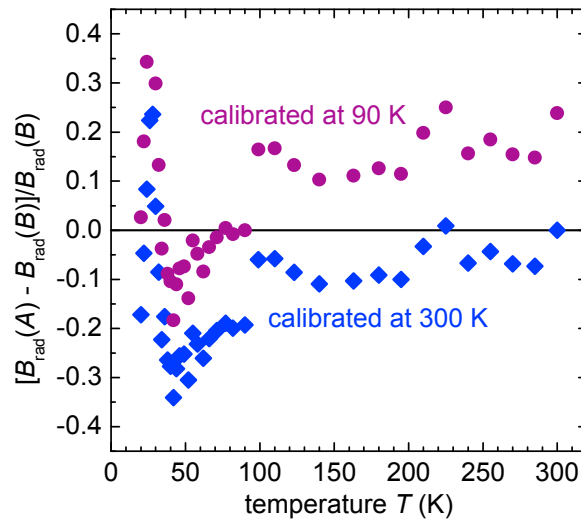

Fig. 5. Relative difference between B_{rad} values derived from samples A and B.

6. Conclusions

We explored a combination of MPL and sPL measurements to determine the radiative recombination coefficient B_{rad} in crystalline silicon, thereby extending the lower limit of the available temperature range from 77 K to 20 K. The T-dependence of B_{rad} can be extracted from the T-dependence of the measured lifetime, determined by MPL via the experimental phase shift with reference to the modulated excitation, and the sPL signal, in combination with numerically determined carrier densities in the dark. Compared to previous determinations of B_{rad} our approach does not require the precise knowledge of the T-dependence of the spectral absorption coefficient or the intrinsic carrier density, both quantities being error-prone at these low temperatures or not available with sufficient accuracy. Errors may be introduced by a possible inequality of differential MPL lifetime and steady-state lifetime. However, the calibration procedure eliminates the related error by calibration with literature values with the benefit that the error issue is reduced to be relevant only if the ratio of the two lifetimes is temperature dependent. Whatever the calibrating temperature chosen at 90 K or at 300 K the relative B_{rad} values show a strong increase by about three orders of magnitude with decreasing temperature from 77 K to 20 K.

Acknowledgements

References

[1] T. Trupke, M. A. Green, P. Würfel, P. P. Altermatt, A. Wang, J. Zhao, R. Corkish, Temperature dependence of the radiative recombination coefficient of intrinsic crystalline silicon. *J. Appl. Phys.* 2003;94:4930.

[2] R. Brüggemann, J. Behrends, S. Meier, S. Tardon, Luminescence, quasi-Fermi levels and applied voltage in ideal and real semiconductor structures. *J. Optoelectron. Adv. Mater.* 2007;9:77–83.

[3] H. T. Nguyen, S. C. Baker-Finch, D. Macdonald, Temperature dependence of the radiative recombination coefficient in crystalline silicon from spectral photoluminescence. *Appl. Phys. Lett.* 2014;104:112105.

[4] M. Ruff, M. Fick, R. Lindner, U. Rössler, R. Helbig, The spectral distribution of the intrinsic radiative recombination in silicon. *J. Appl. Phys.* 1993;74:267.

[5] R. Brüggemann, S. Reynolds, Modulated photoluminescence studies for lifetime determination in amorphous-silicon passivated crystalline-silicon wafers. *J. Non-Crystal. Solids* 2006;352:1888-1891.

[6] P. Würfel, The chemical potential of radiation. *J. Phys. C: Solid State Phys.* 1982;15:3967.

[7] P. Würfel, S. Finkbeiner, E. Daub, Generalized Planck's radiation law for luminescence via indirect transitions. *Appl. Phys. A* 1995;60:67-70.

[8] T. Trupke, E. Daub, P. Würfel, Absorptivity of silicon solar cells obtained from luminescence. *Sol. Energy Mater. Sol. Cells*. 1998;53:103-114.

[9] R. Brüggemann, M. Xu, J. Alvarez, M. Boutchich, J.-P. Kleider, Temperature dependence of the radiative recombination coefficient in crystalline silicon by spectral and modulated photoluminescence. *Phys. Status Solidi RRL* 2017:1700066.

[10] D. K. Schroder, *Semiconductor Material and Device Characterization*. New York: Wiley, 1990.

[11] J. A. Giesecke, S. W. Glunz, W. Warta, Understanding and resolving the discrepancy between differential and actual minority carrier lifetime. *J. Appl. Phys.* 2013;113:073706.

[12] F. Werner, W. Stals, R. Görtzen. B. Veith, R. Brendel, J. Schmidt, High-rate atomic layer deposition of Al_2O_3 for the surface passivation of Si solar cells. *Energy Procedia* 2011;8:301.

[13] J. Schmidt, F. Werner, B. Veith, D. Zielke, S. Steingrube, P. P. Altermatt, S. Gatz, T. Dullweber, R. Brendel, Advances in the Surface Passivation of Silicon Solar Cells. *Energy Procedia* 2012;15:30.

[14] S. Dauwe, J. Schmidt, R. Hezel, Very low surface recombination velocities on p- and n-type silicon wafers passivated with hydrogenated amorphous silicon films. *29th IEEE PV Specialist Conference (PVSC)*, 20 - 24 May 2002, New Orleans, USA, Piscataway: IEEE; 2002. p. 1246.

[15] F. Werner, B. Veith, D. Zielke, L. Kühnemund, C. Tegenkamp, M. Seibt, R. Brendel, J. Schmidt, Electronic and chemical properties of the c-Si/Al_2O_3 interface. *J. Appl. Phys.* 2001;109:113701.